Autonomous Golf-Ball Recollection System

Team Members: Jonathan Farrow, David Perkins, Scott Rahim

Class: ME 4041

Professor: Yan Wang

Table of Contents

Contents

Introduction

The product under design is an autonomous robot that can collect and store golf balls, and is based on a stock model of a Tango E5 autonomous lawn-mowing robot made by John Deere. On the back of the robot, a revolving picker will be attached so that golf balls can be picked up from the ground. The picker is currently an extremely popular method of picking up and storing golf balls, but is usually required to be manually operated. The picker is made up of disks that wedge golf balls into circular channels for placement inside a storage unit. A hopper will be placed on the picker trailer for the collection of the golf balls. The hopper will have teeth that will lie in the path of the embedded golf balls to remove them from the channels for storage within the hopper.

The product was chosen to reduce the expense of picking up golf balls currently experienced by owners of large driving ranges, who usually employ tractors and hired labor for golf ball collection. The owner currently has to pay for the initial cost of the trailer, pay for gas, as well as an employee for operation of the tractor. Finally, the owner of the driving range must also make sure that the tractor is receiving adequate maintenance to ensure that operation is at its best. The autonomous golf ball collector that is being proposed will reduce most of the above costs and eliminate some completely. The initial cost of the autonomous robot will not cost nearly as much as a tractor will, and the cost of running the robot will be significantly less than a tractor. The robot will also be able to eliminate the need for the owner to pay someone to operate the tractor, and will only have to pay for the charging of the robot. Maintenance of the robot will also be required, but the time and money spent on maintenance of the robot will be far less than the time and money spent on the maintenance of the tractor. Overall, the autonomous golf ball collection robot will provide a much cheaper method for collecting golf balls on a driving range.

Objectives

The main objective for the design of the autonomous golf ball recollection system was to create a joint effort between existing technologies to make an affordable robot that would successfully collect and store golf balls. It was decided that the project needed to be split into two areas, one focusing on a current robot that could be modified to collect golf balls and a golf ball collection system .The Tango E5 autonomous lawn mower by John Deere was chosen as the initial design for the robot. Modifications needed to made so that translation between mowing lawns to golf ball recollection could be made. A golf ball picker design was chosen as the method for the actual collection of golf balls due to its proven ability to collect large quantities of golf balls with little error. Once the robot and collection system had been determined, modifications to both system need to be made so that a joint effort between John Deere and a golf ball picker company can be realized as a feasible and profit producing project.

Modeling

Below, the main parts that needed to be modeled for the autonomous golf ball collection system are displayed, as well as the methods used to model said parts. NX was used as the program of choice for the CAD models.

Top Shell.

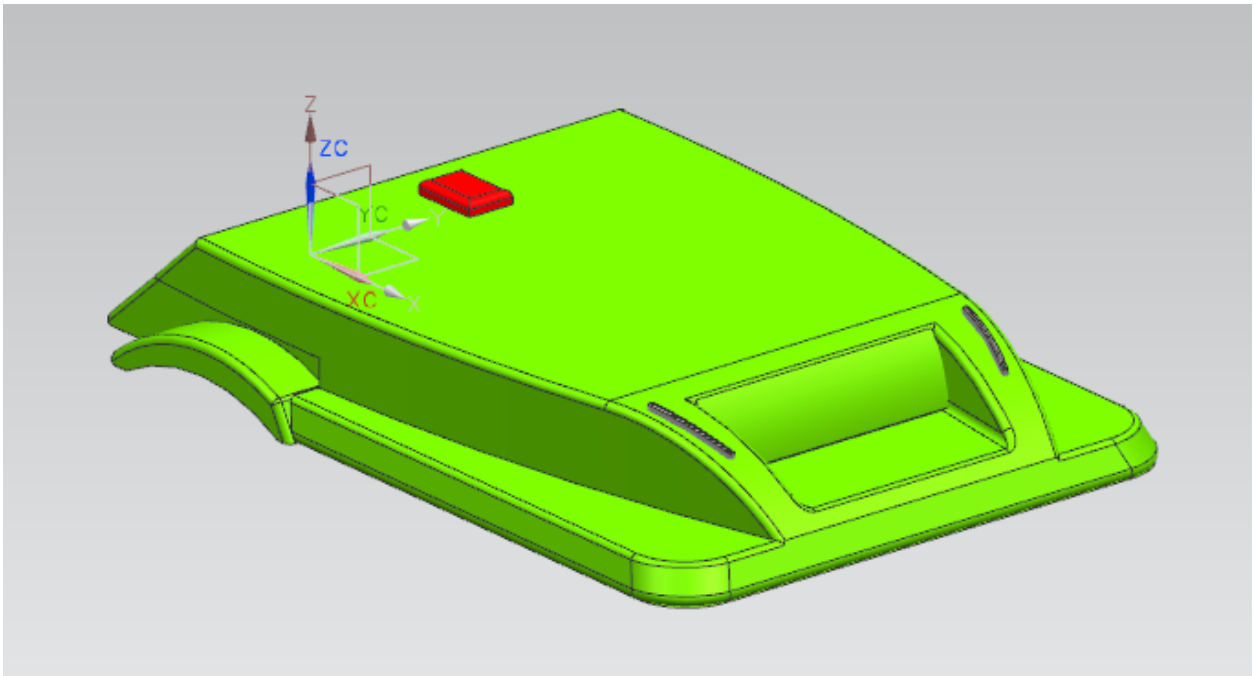

Figure 1. Top Shell of Tango

Figure 1 shows the top view of the top shell. Also shown are the charging points and the emergency stop button, which is the red button on top of the shell. The placement of the charging points was determined by taking the size, shape, and connection points of the charging station into consideration. This component was designed by sketching a box, and then extruding it to meet the dimensions of the actual robot. Material was extruded at an angle on the bottom portion of the top shell to provide the sloped surface seen above. The mirror command was also used on features, such as the charging points, that are on both sides of the shell. Lastly, edge blend was used to smooth out the edges of the shell.

Bottom Shell.

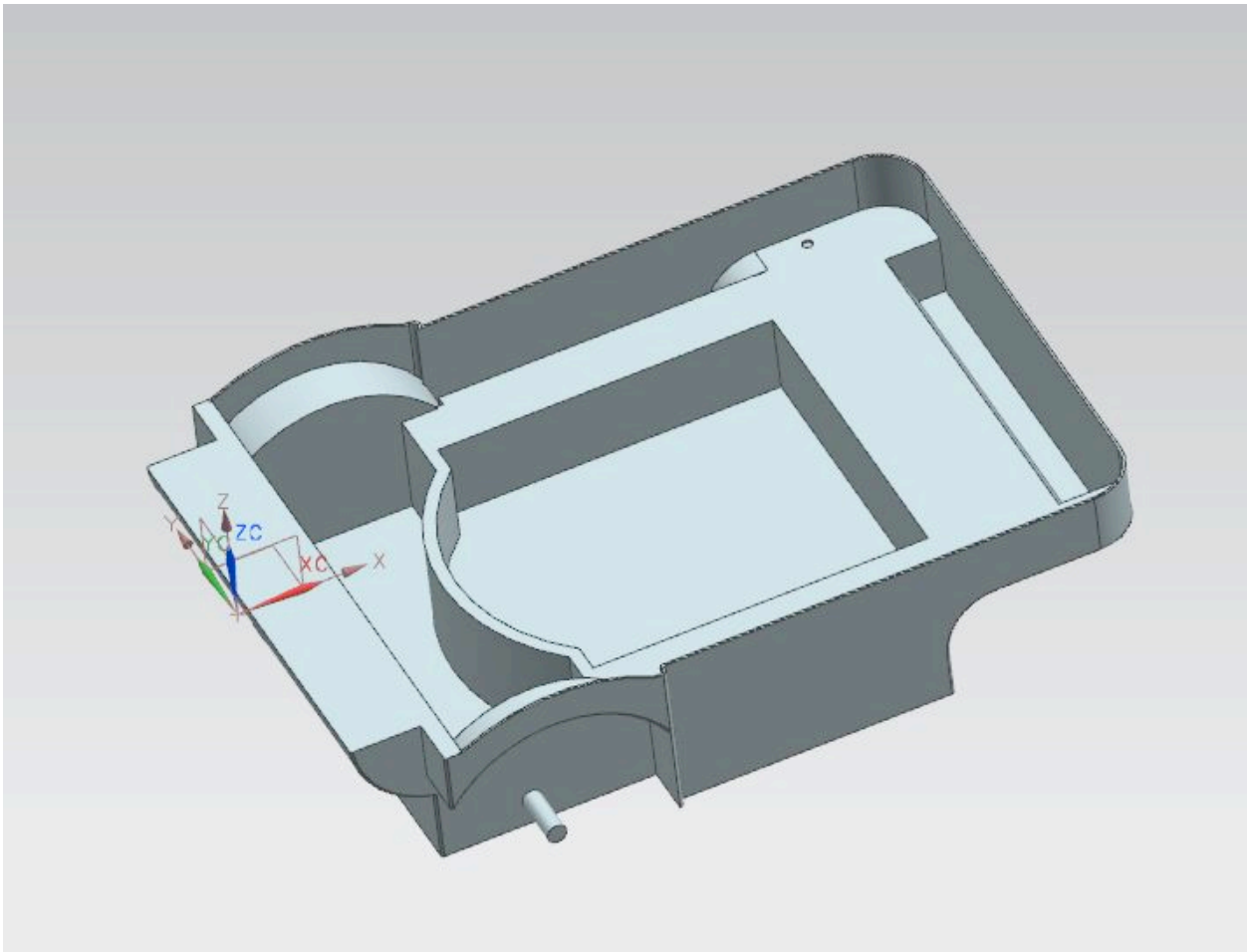

Figure 2. Bottom Shell of Tango

Figure 2 shows the top view of the bottom shell, which connects with the top shell to hold the motor for the robot. This component was designed taking the dimensions of the top shell into consideration in order to ensure a perfect fit for final assembly. Once again this part was designed by first sketching a box and extruding it to meet the shape and dimensions of the actual bottom shell of the robot. The mirror feature was utilized on points that exist on both sides of the shell. Additionally, edge blend was used to smooth out the edges of the part.

Back Wheels.

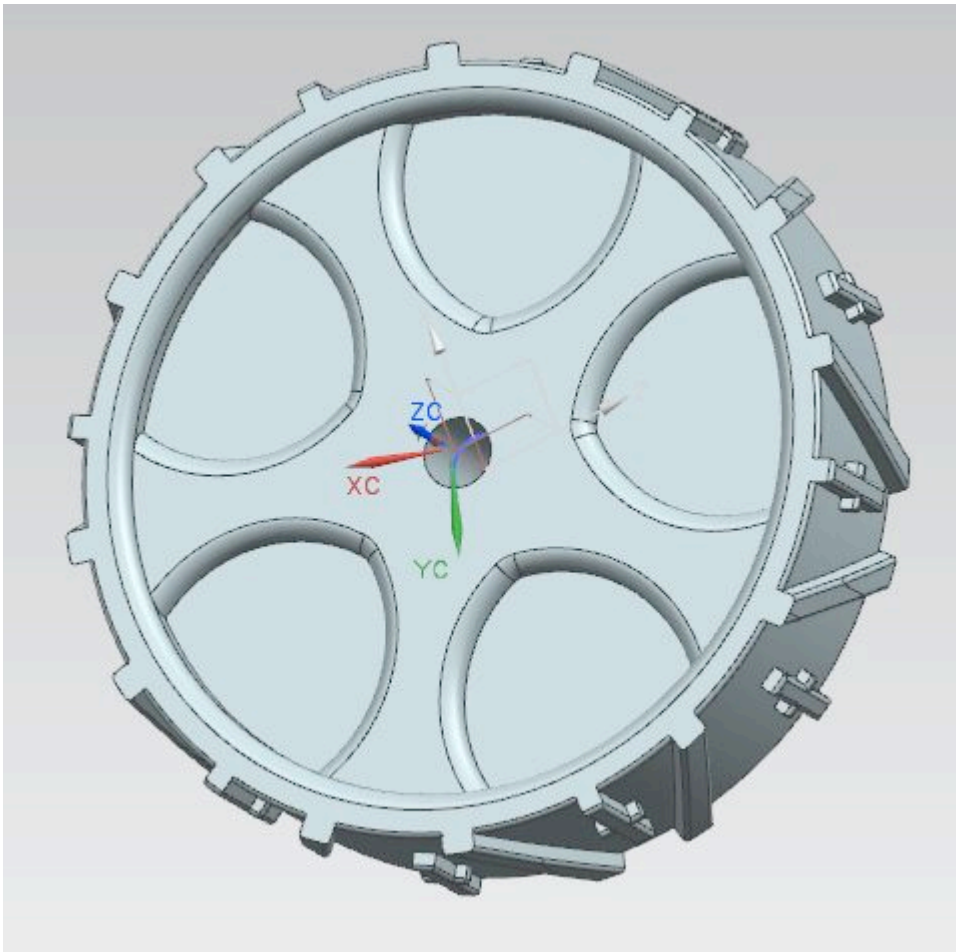

Figure 3. Back Wheels of Tango

Figure 3 shows the back wheels for the robot. This wheel was designed by sketching a circle and extruding it to the actual depth of the robot wheel. Additional features were sketched to make our model a better representation of the actual wheel. The pattern option was used on to copy the tread design around the outside of the wheel. The pattern feature was also used to form the shape of the outside facing wall of the wheel. Lastly edge bend was used to smoothen out the edges.

Front Wheels.

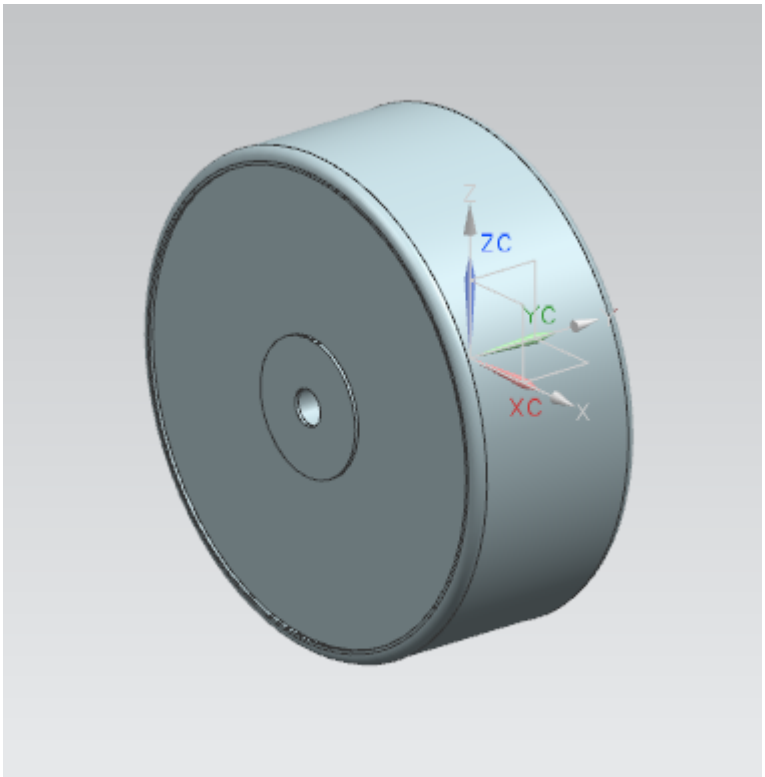

Figure 4. Front Wheel

Figure 4 shows the front wheel of the robot. Once again, this component was designed by sketching a circle and extruding it to meet the depth of the actual front wheel of the robot. Edge blend was used to smoothen out the edges.

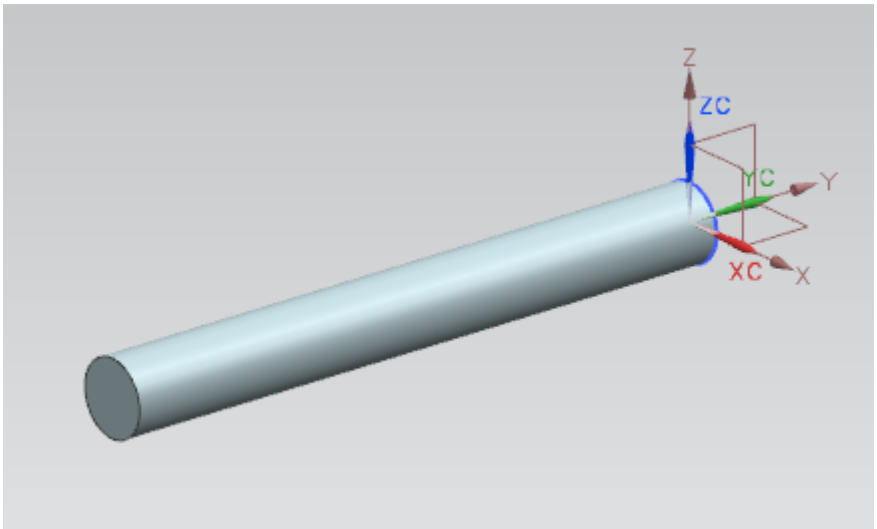

Figure 5. Connection Pin for Front Wheels

Figure 5 shows the pin that connects the front wheels to their respective brackets. This part was designed by simply sketching a circle with a diameter similar to the actual pin and extruding it.

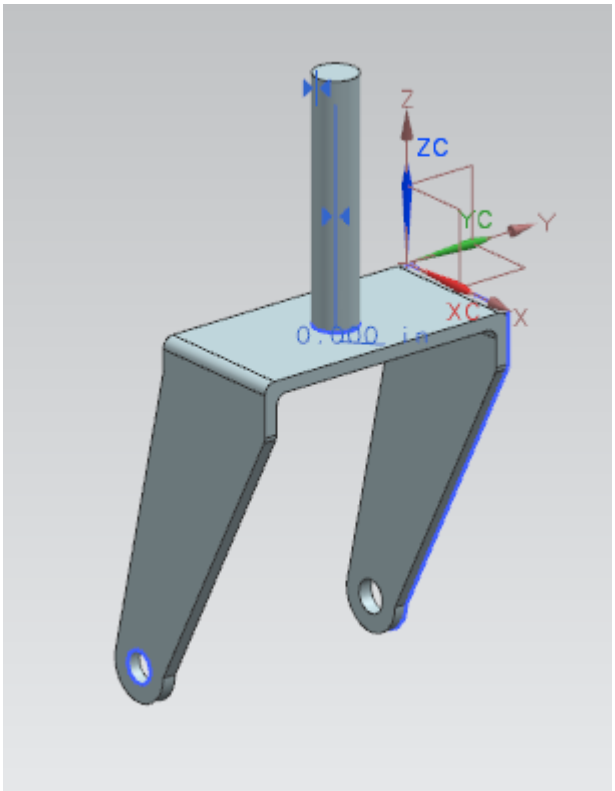

Figure 6. Front Wheel Offset Bracket with Connection Pin

Figure 6 shows the front wheel bracket. The purpose of the bracket is to hold on to the wheel and keep it attached to the robot. This component was designed by sketching a rectangle and extruding it to meet the actual dimension and shape of the wheel bracket. The sloped sides of the bracket were made by creating a datum plane perpendicular to the desired direction of extrusion. A circle was extruded from the top surface of the bracket so that connection can be made between the front wheel assembly and the robot.

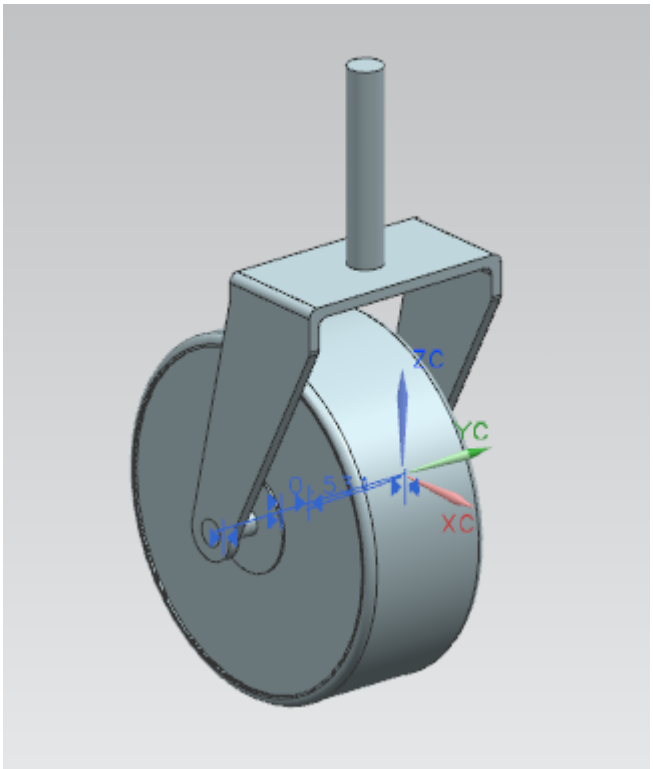

Figure 7. Front Wheel Fully Assembled

Figure 7 shows the full assembly of the front wheel, connection pin, and front bracket.

Motor for Back Wheel.

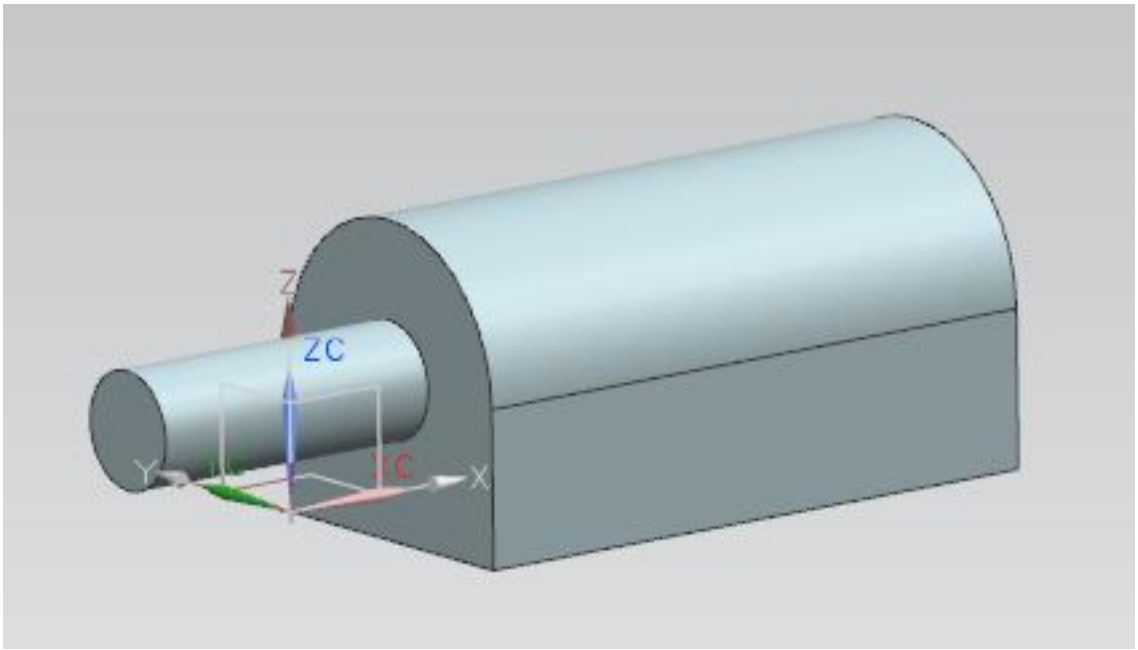

Figure 8. Motor for Back Wheel

Figure 8 shows a representation of the final motor that will be in the Tango robot, which produces the power for the robot to do its job. It is placed inside the bottom shell, on top of the back wheels. This part was created by sketching a rectangle and extruding it to a similar shape to an actual motor. Then, a circle was sketched on one of the sides and extruded to represent the component that comes out of the side of the motor.

Fully Assembled Tango Robot.

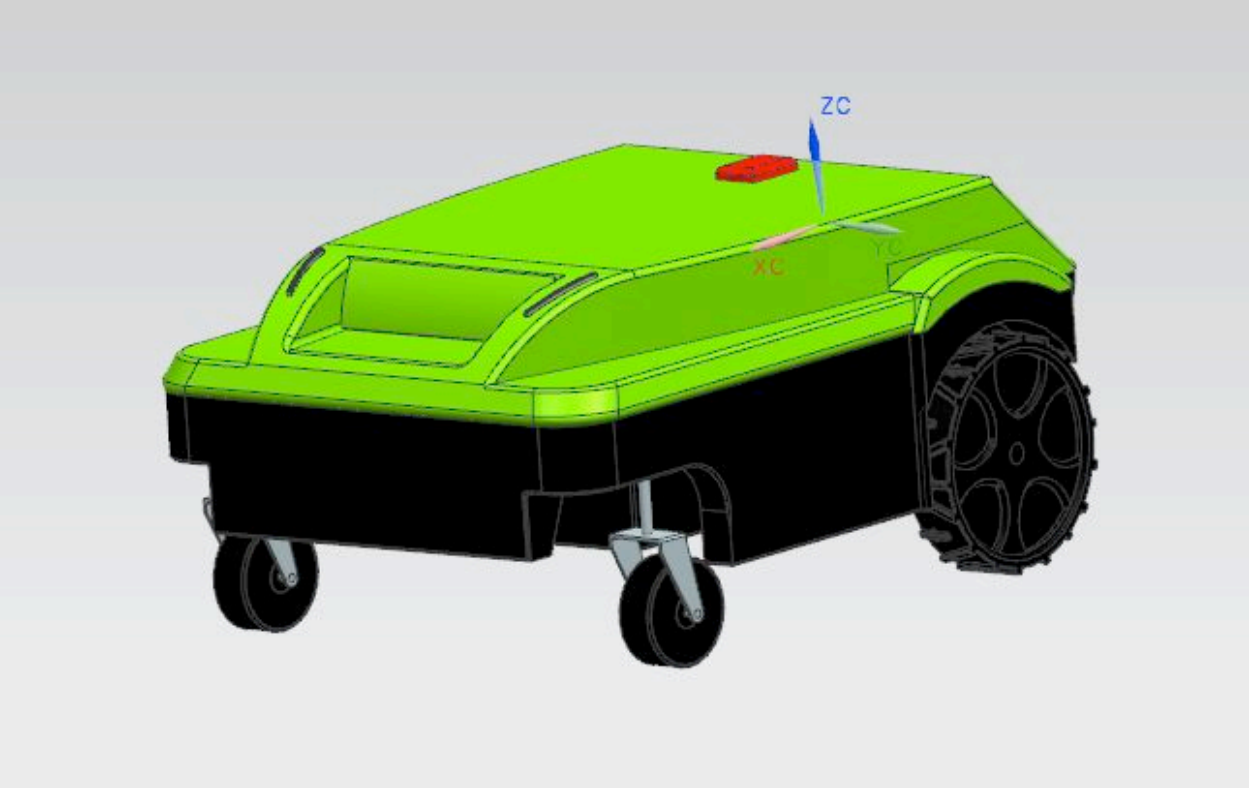

Figure 9. Fully Assembled Tango Robot

Figure 9 shows the full assembly of the robot without the trailer.

Ball Remover.

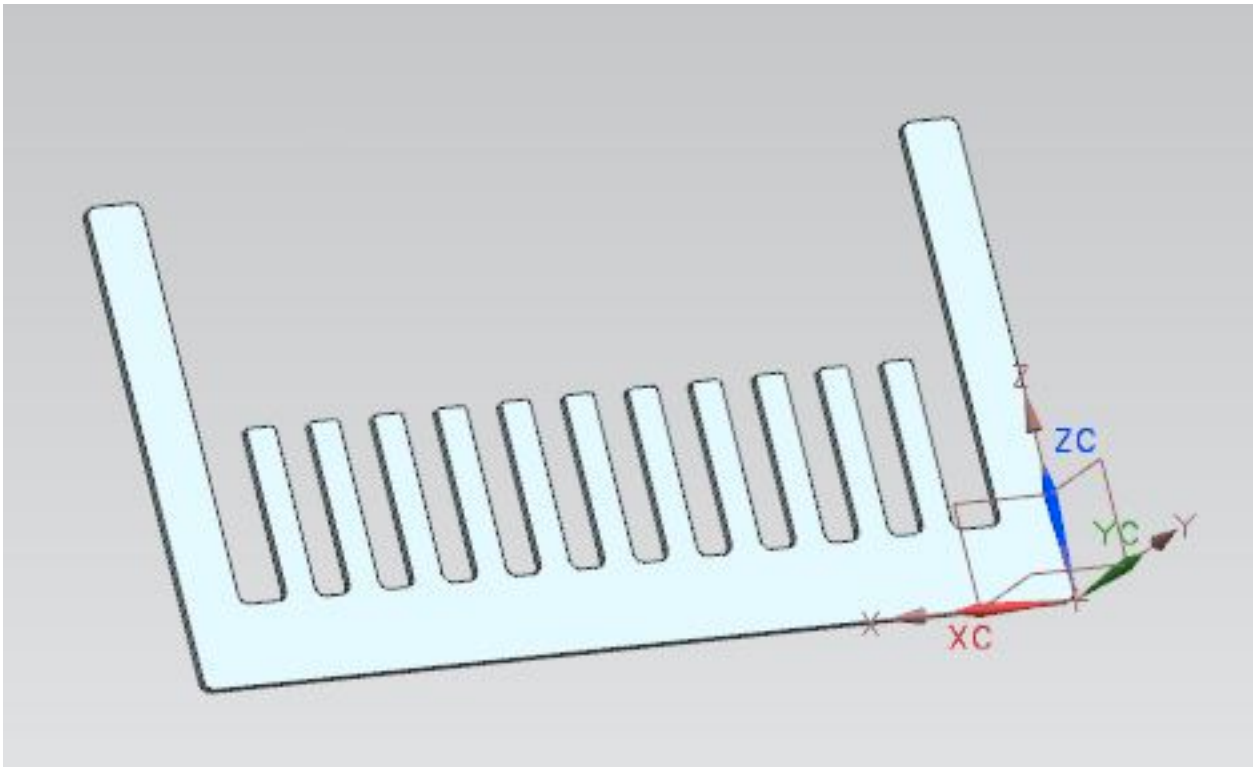

Figure 10. Ball Remover

Figure 10 shows the component that removes the golf balls after they have been picked up. The part was made by first creating the outer U-shaped portion, without the picker teeth. by measuring the desired distance in between picker disks, one tooth of the part was created and then arrayed across to complete the part. Edge blend was used to smooth out edges and reduce any stress the picker teeth might feel during golf ball collection.

Basket.

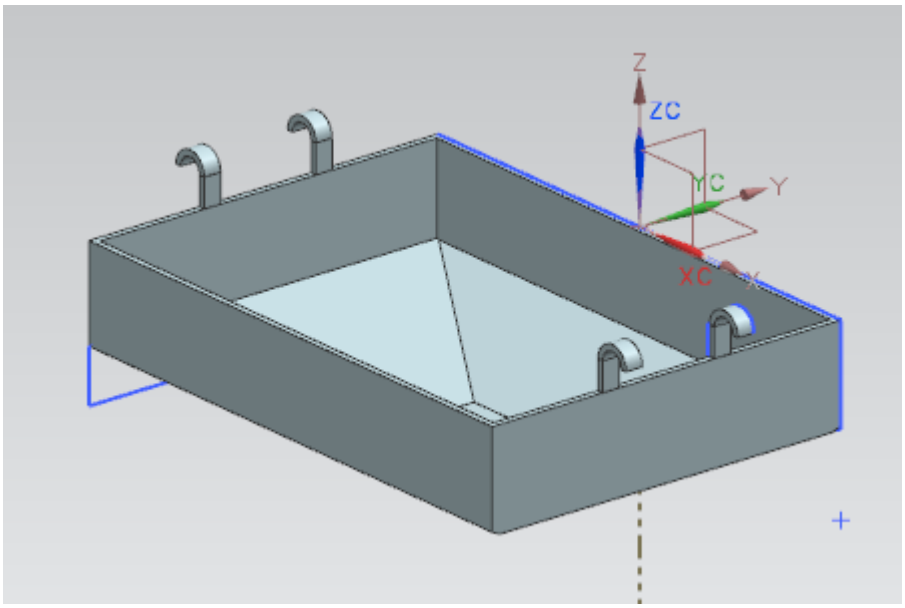

Figure 11. Basket for Ball Storage

Figure 11 shows the storage unit for the golf balls during collection. The part was first crafted by created a square sketch and extruded to the desired height of the basket. The basket then had sides of the rectangle subtracted, so that the inside of the basket would be able to funnel the balls to the bottom. Finally, the shell feature was utilized to make the basket hollow. Once the actual basket had been crafted, the hooks for attaching to the robot needed to be modeled. The side of the basket was used as the sketch plane, where the hook design was crafted to lie along the edge of the top portion of the basket. The desired distance from the side of the basket was determined and the hook was the extruded. The array feature was used to copy the feature and place it at a similar distance along the same edge. Finally, the mirror feature was used to copy the hooks onto the opposite side of the basket.

Bearing For Picker Disks.

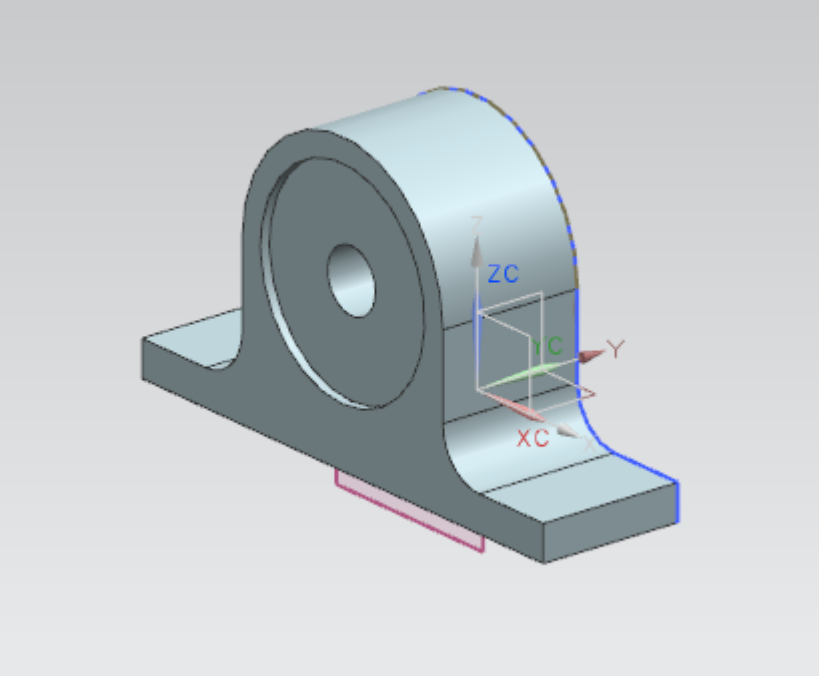

Figure 12. Bearing Used for Rotation of Picker Disks

Figure 12 shows the bearing used for rotation of the picker disks. The outline of the bearing was sketched onto a plane, with a circle in the middle being left out of the extrusion for connection with the center rod that held the picker disks together, and then extruded to the desired distance. The center circle was offset in another sketch on the outside face of the bearing, and then subtracted slightly from the solid to represent the actual bearing itself. This subtraction was then mirrored onto the other surface face using a datum place placed at the center of the part. Edge blend was used to smooth out the bearing surfaces.

Connection For Pipes to Bearing.

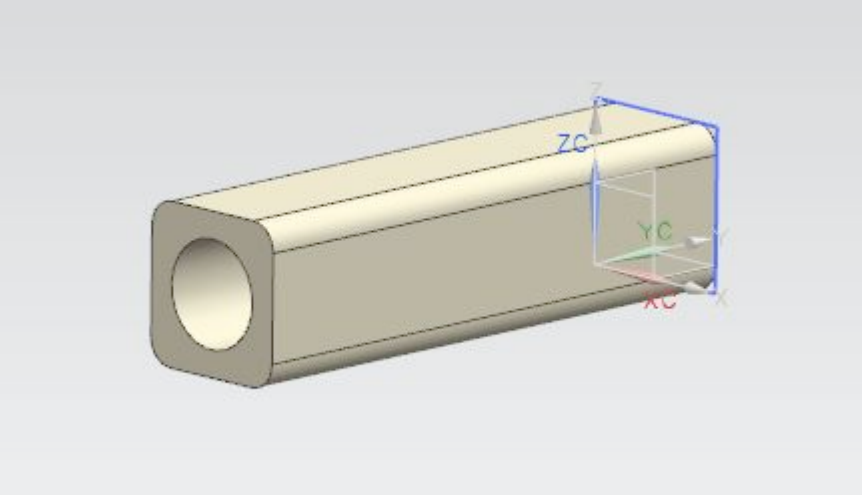

Figure 13. Connector For Pipe Bearing to Side Rods

Figure 13 shows the component that connects the side pipes of the robot to the bearing. This part was created by sketching a square with a hole about its center with dimension similar to the actual connector, and then extruding it. Edge blend was curve the outside edges.

Bearing For Trailer and Robot Connection.

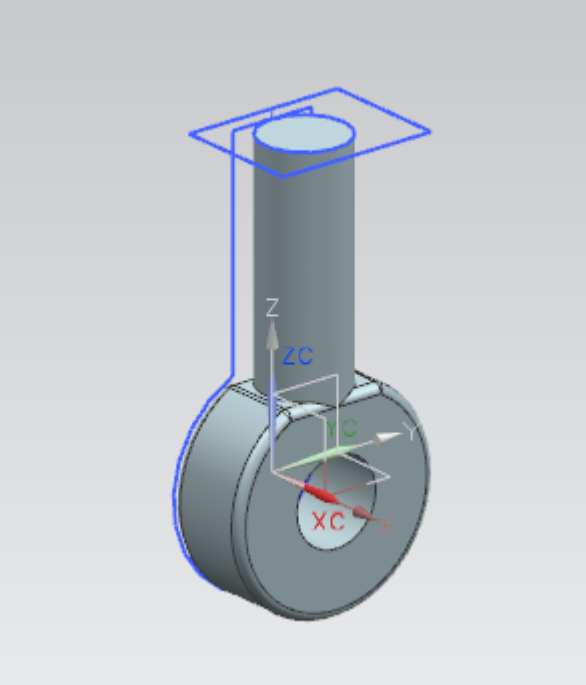

Figure 14. Bearing for Connection of Picker Trailer to Tango

Figure 14 shows the bearing that connects the picker trailer to the Tango. The circular part of the bearing was first modeled, with a hole in the middle for connection to the trailer. The top portion of the circle was then subtracted to create a flat surface. The flat surface was used as a sketch plane, where a cylinder was extruded to connect the trailer to the robot. Edge blend was used to reduce an stress that the part may feel by reducing any rapid changes in width along the part.

Front and Side Rods.

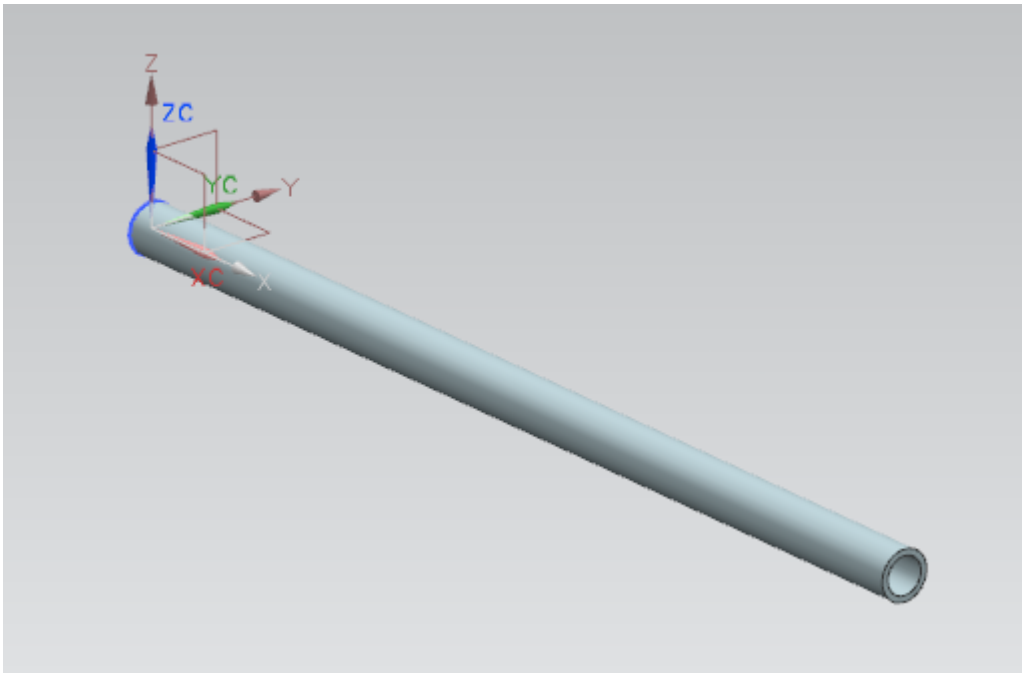

Figure 15. Front Rod of Trailer

Figure 15 shows the front rod of the trailer. A circle was sketched with a diameter similar to the actual rod, and then extruded.

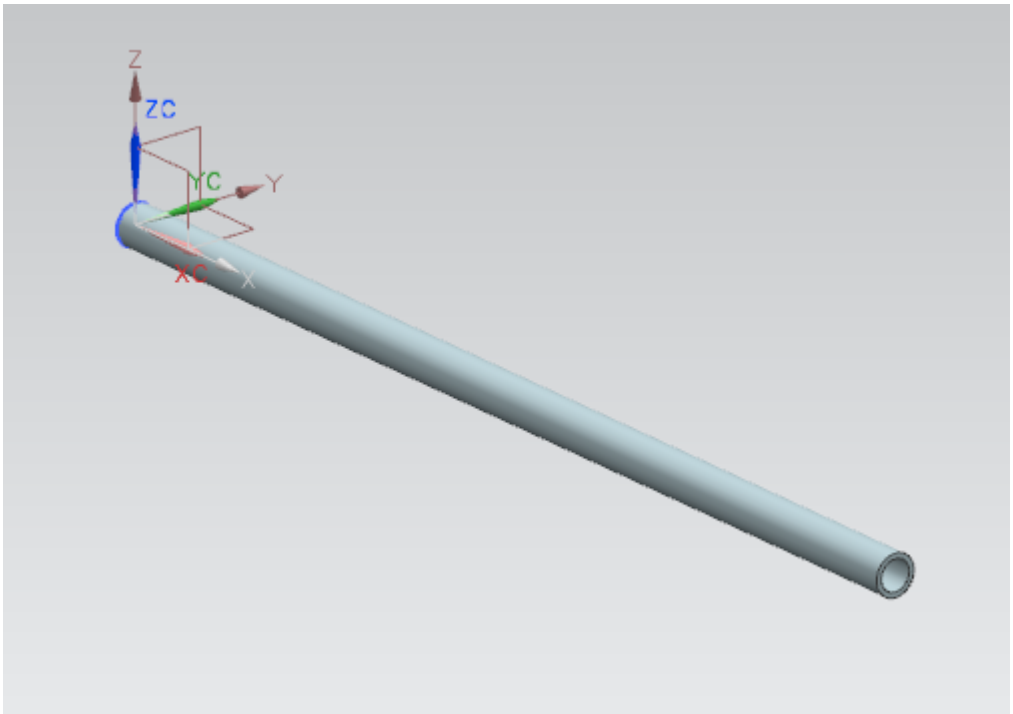

Figure 16. Side Rods of Trailer

Figure 16 shows one of the side rods of the trailer. This part was made the same way as the component shown in Figure 15.

Elbow for Front and Side Rod Connection.

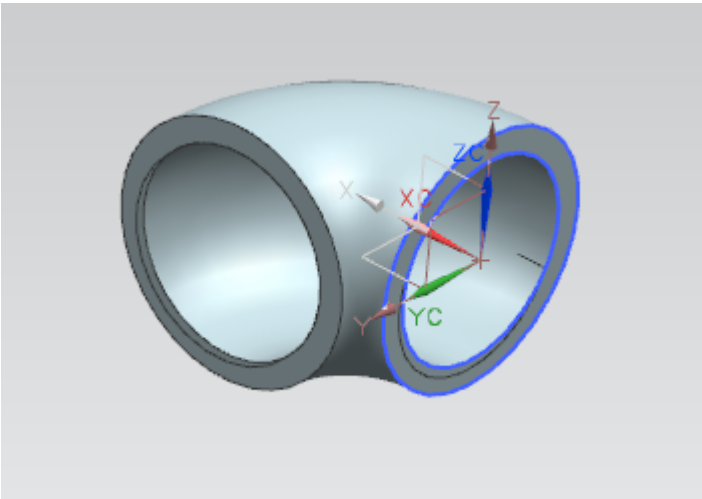

Figure 17. Elbows for Connection of Side Rods and Front Rod

Figure 17 shows the elbow that connects the front and side rods together. The part was created by making a circular sketch using the origin datum axes, and then revolved 90 degrees.

Pipe Through Picker Disks.

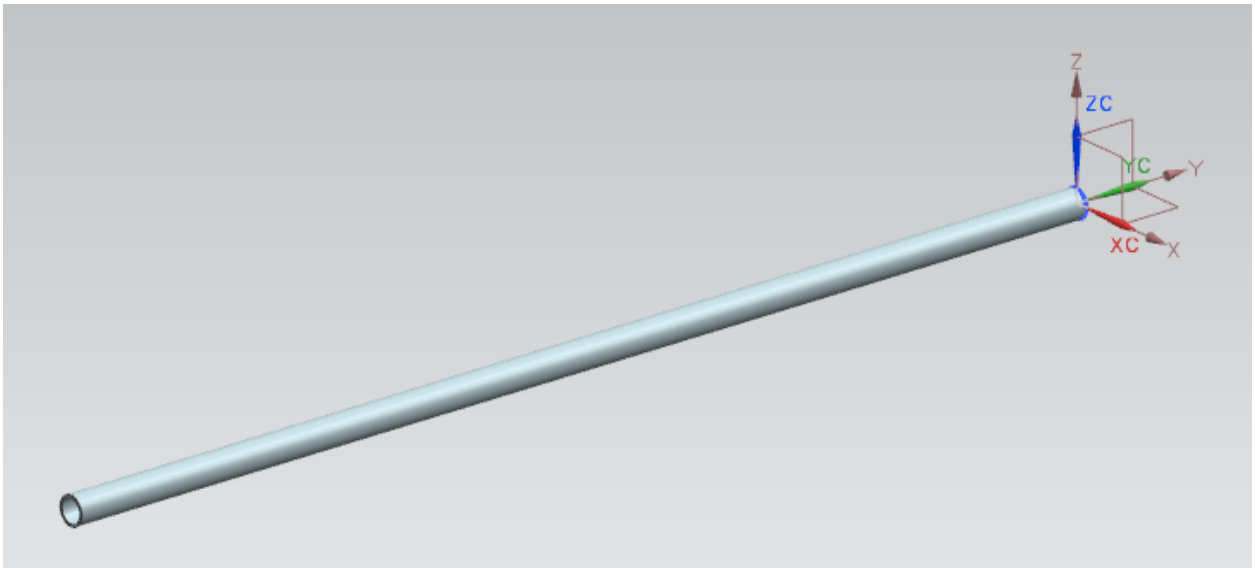

Figure 18. Pipe Through Picker Disks

Figure 18 shows the pipe that goes through the roller disks, which pick up the golf balls, and connects them together. Once again, this part was made by sketching a circle and extruding it to the length of the actual pipe.

Roller Disk (Normal and End).

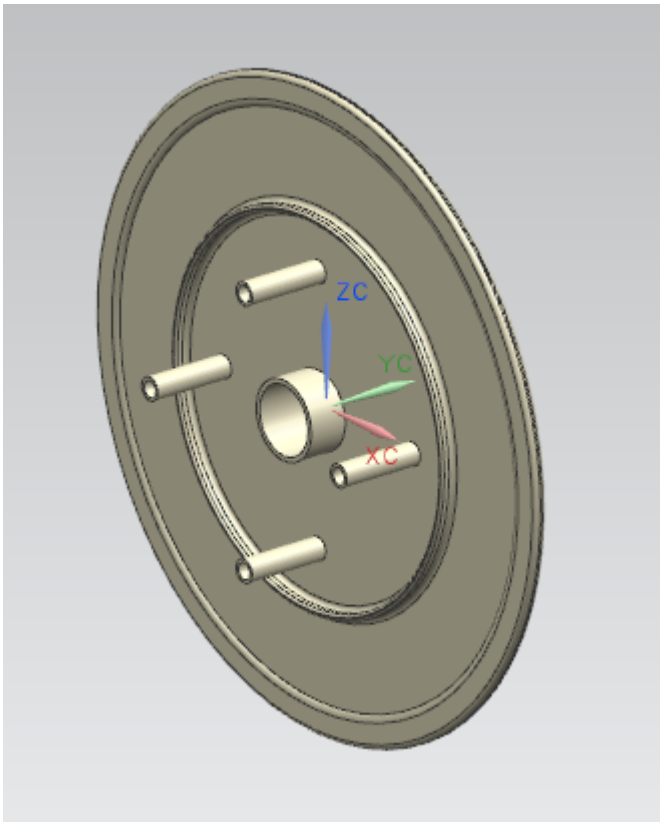

Figure 19. Roller Disk Used for Golf Ball Collection

Figure 19 shows one of the roller disks used for golf ball collection. A circle was first extruded to get the maximum width of the picker disks established. An inner channel was created by offsetting the first circle twice in a sketch and subtracting from the surface. A cylinder was extruded in the center of the disk with a hole in the for the pipe seen in Figure 18. A single cylinder was created around the center cylinder that would meld the disks together. This cylinder was then patterned around the center to create the four cylinders seen.

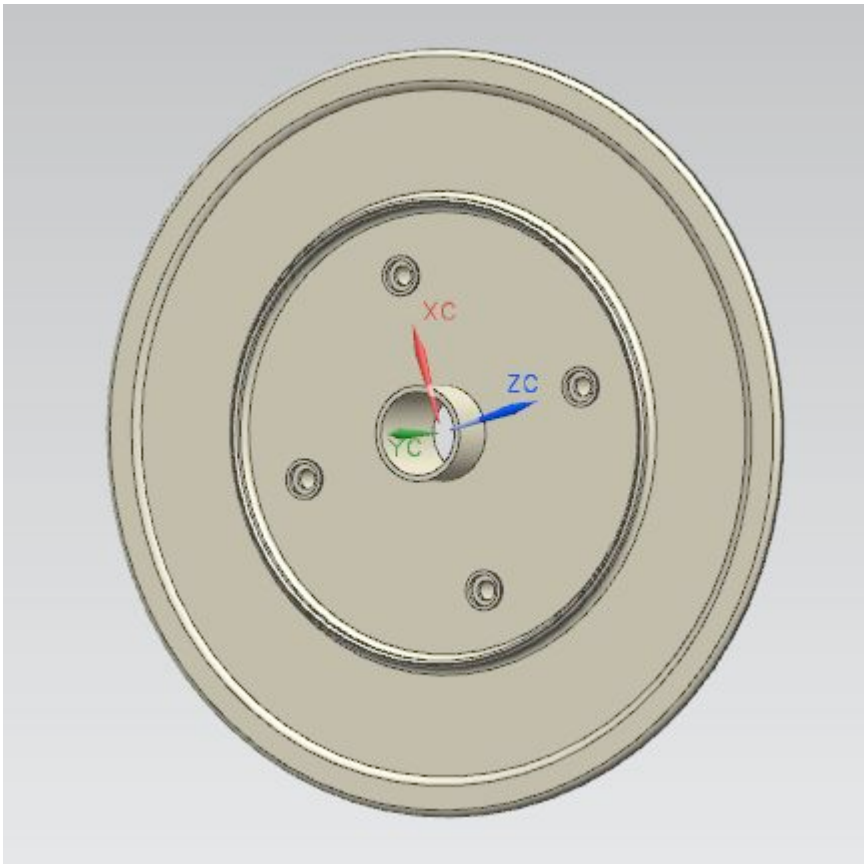

Figure 20. End Roller Disk

Figure 20 shows the back of the disk seen in Figure 19. The majority of the features were mirrored to the back side, save for the four cylinders. Instead, small holes were created so that the disks could be linked together.

Fully Assembled Trailer.

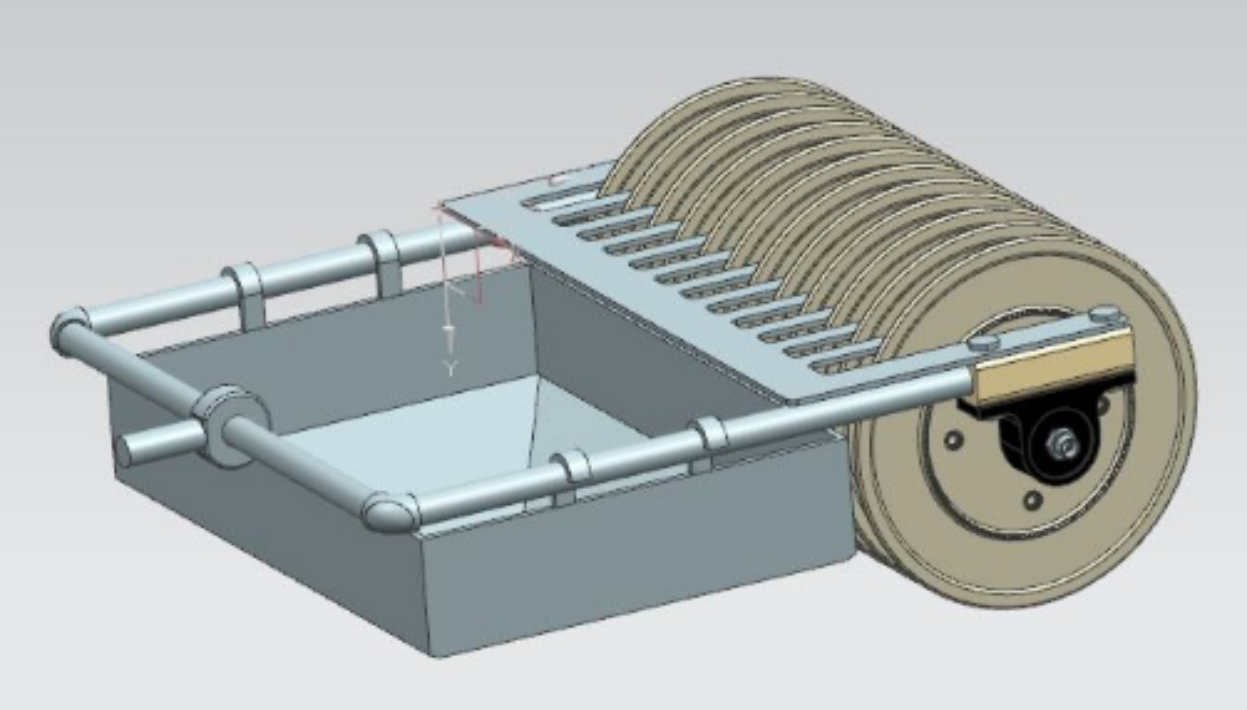

Figure 21. Trailer Fully Assembled

Figure 21 shows the trailer by itself, fully assembled. Parts include the bearing to the robot, bearing for the roller disks, 12 assembled roller disks, the ball remover, and the basket.

Charging Station.

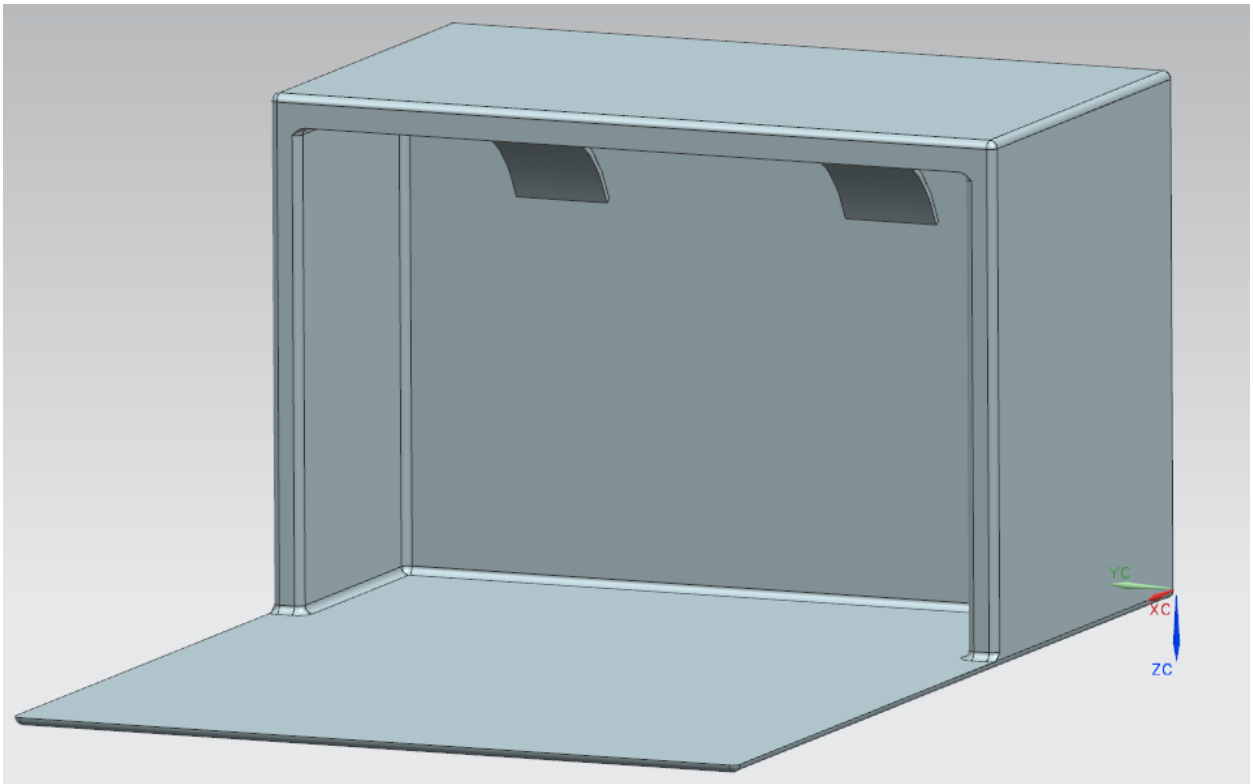

Figure 22. Charging Station for Tango

Figure 21 shows the charging station for the robot. This part was created by sketching a rectangle and extruding it to match the dimensions and shape of the actual charging station. The pedals shown inside the station are the features that charge the robot.

Fully Assembled Robot and Charging Station.

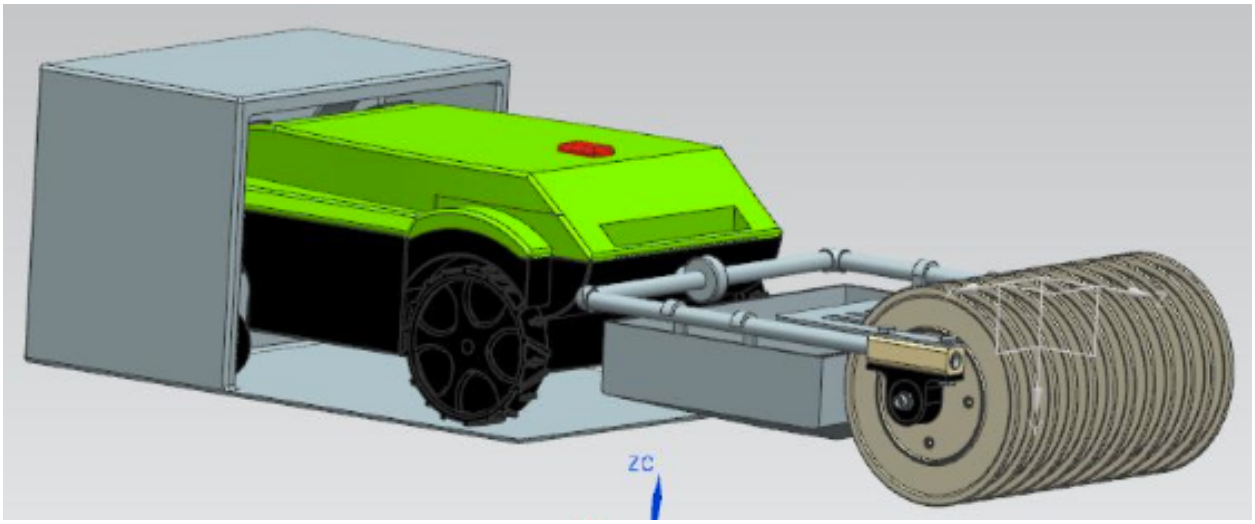

Figure 23. Robot Full Assembly and Charging Station

Figure 23 shows the whole assembly of the robot, trailer and charging station.

Analysis and Verification:

FEA Analysis 1.

FEA analysis was performed on three separate areas on the robot to ensure that each piece was able to handle any stresses it may encounter while running. The first area of focus is the bearing that connects the trailer of the golf ball collector to the actual robot as seen in Figure 23,

Figure 23. Connection Between Golf Ball Collector Trailer and Tango Robot

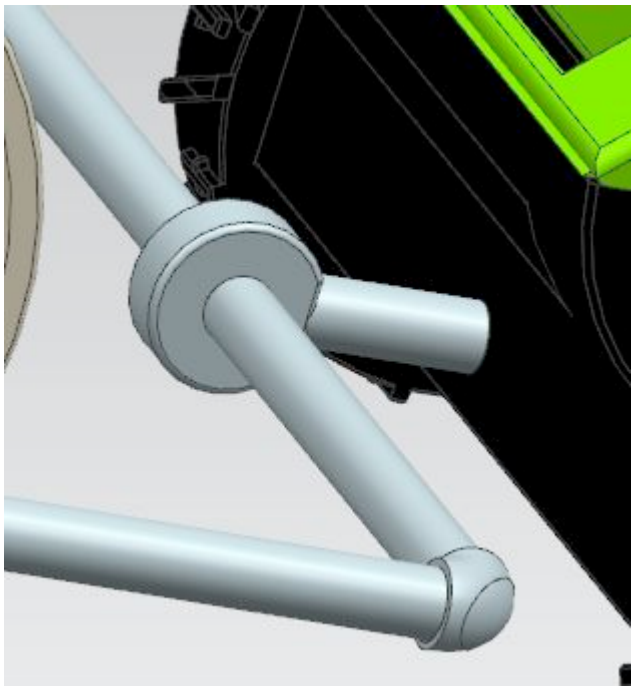

FEA was first performed by hand so that validation between theory and the NX solution solver could be verified. The force encountered by the bearing was determined to be the force to overcome friction that the trailer would encounter, as seen in Eq. 1,

$$F = \mu N \tag{1}$$

where F is the force of friction, μ is the coefficient of friction, and N is the normal force provided by the trailer and is equivalent to the combined weight. First, the weight of the trailer needed to be added to the weight of the maximum amount of golf balls the trailer can hold at one time. The mass of the trailer was determined to be roughly 27.6 kg and the mass of 200 golf balls was found to be 9.2 kg, for a total weight of 360.64 N, or 81.08 lb-f. The coefficient of friction for a car wheel on grass was discovered to be roughly 0.35, and was assumed to be nearly the same for the picker disks on the robot. The frictional force was determined to be 126.2 N, or 28.37 lb-f.

Once the force that would be acting on the member was determined, the next portion of calculations involved using FEA to determine how much the member deformed. Assuming that the bearing was similar to a cantilever beam, with the bearing end being fixed, Eq. 2 was used to determine the change in length axially,

$$\begin{bmatrix} F_1 \\ F_2 \end{bmatrix} = \begin{bmatrix} k & -k \\ -k & k \end{bmatrix} * \begin{bmatrix} d_{1x} \\ d_{2x} \end{bmatrix} \tag{2}$$

where F1 is the reaction force, F2 is the force from friction, or 28.37, d_{1x} is the displacement at the bearing and assumed to be zero, d_{2x} is the displacement at the connection point of the robot, and k is calculated by using Eq. 3,

$$k = \frac{EA}{L} \tag{3}$$

where E is young's modulus, A is the surface area of the plane perpendicular to the force, and L is the length of the member. Setting the material properties of the bearing to steel, E was found to

be 30 Mpsi, A was determined to be 0.785 in^2, and L was found to be 2.65 in. K was then calculated to be $8.9*10^6$ lb/in. d_{2x} can then be determined and was calculated to be $3.0*10^{-6}$ in. Do to the bearing body being fairly thick with respect to its height, the Plane Strain FEA equations were used to determine the stress encountered by the bearing, Eq. 4 was used,

$$\begin{bmatrix}\sigma_x\\ \sigma_y\\ \tau_{xy}\end{bmatrix} = \frac{E}{(1+v)(1-2v)}\begin{bmatrix}1-v & v & 0\\ v & 1-v & 0\\ 0 & 0 & \frac{1-2v}{2}\end{bmatrix} * \begin{bmatrix}\varepsilon_x\\ \varepsilon_y\\ \gamma_{xy}\end{bmatrix} \tag{4}$$

where σ is the axial stress, τ_{xy} is the shear stress, v is poisson's ratio for steel (0.29), ε is the engineering strain, and γ_{xy} is the shear strain, which is assumed to be zero in this situation. ε_x is calculated by using Eq. 5

$$\varepsilon_x = \frac{d_{1x}}{L} \tag{5}$$

and was determined to be 1.0×10^{-6}. ε_y is determined by using Eq. 6,

$$\varepsilon_y = -\varepsilon_x v \tag{6}$$

and was determined to be -3.5×10^{-7}. By plugging in the solved values into Eq. 4,

$$\begin{bmatrix}\sigma_x\\ \sigma_y\\ \tau_{xy}\end{bmatrix} = \begin{bmatrix}34.71 psi\\ 3.64 psi\\ 0\end{bmatrix}$$

where the stress encountered by the bearing is well within steels limits.

After validating by hand, NX was used to create a more complex model of the force, as can be seen in Figure 24,

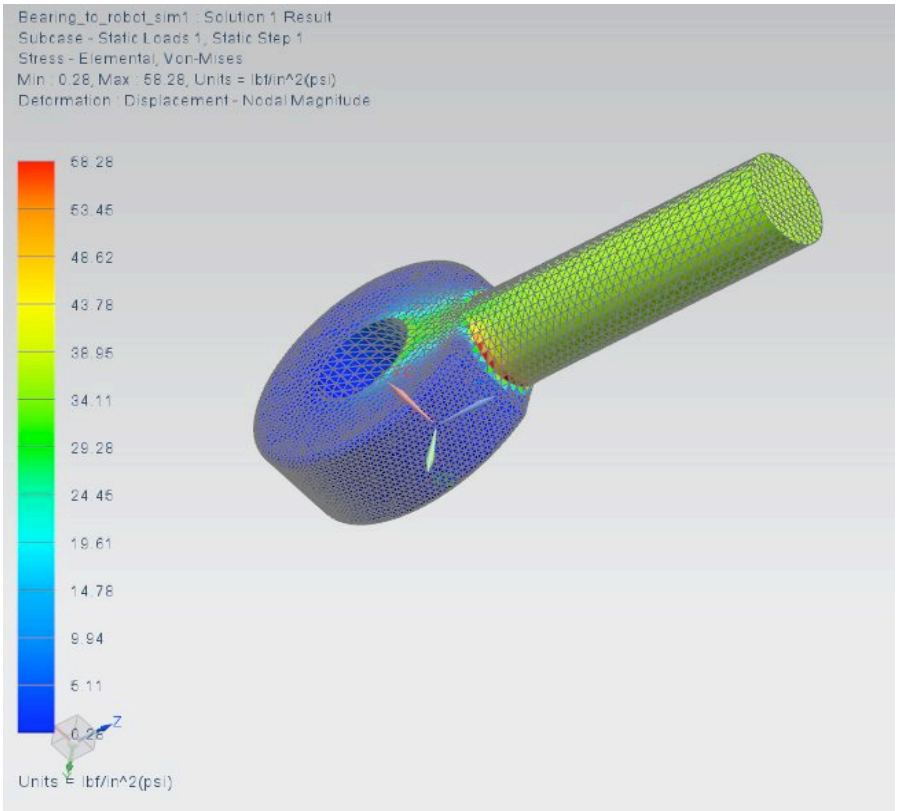

Figure 24. Stress Analysis Performed on Bearing

Comparison between NX solution and hand FEA solutions are very close, with the stress along the member being between 34.11 and 36.95 psi. Stress does increase close to the curvature of the bearing, which is expected but not accounted for in the hand comparison of the FEA process.

FEA Analysis 2.

The second area of focus for FEA analysis was the stress encountered by the deflection of a single picker disk while collecting a golf ball. An example of the picker disk can be seen below in Figure 25,

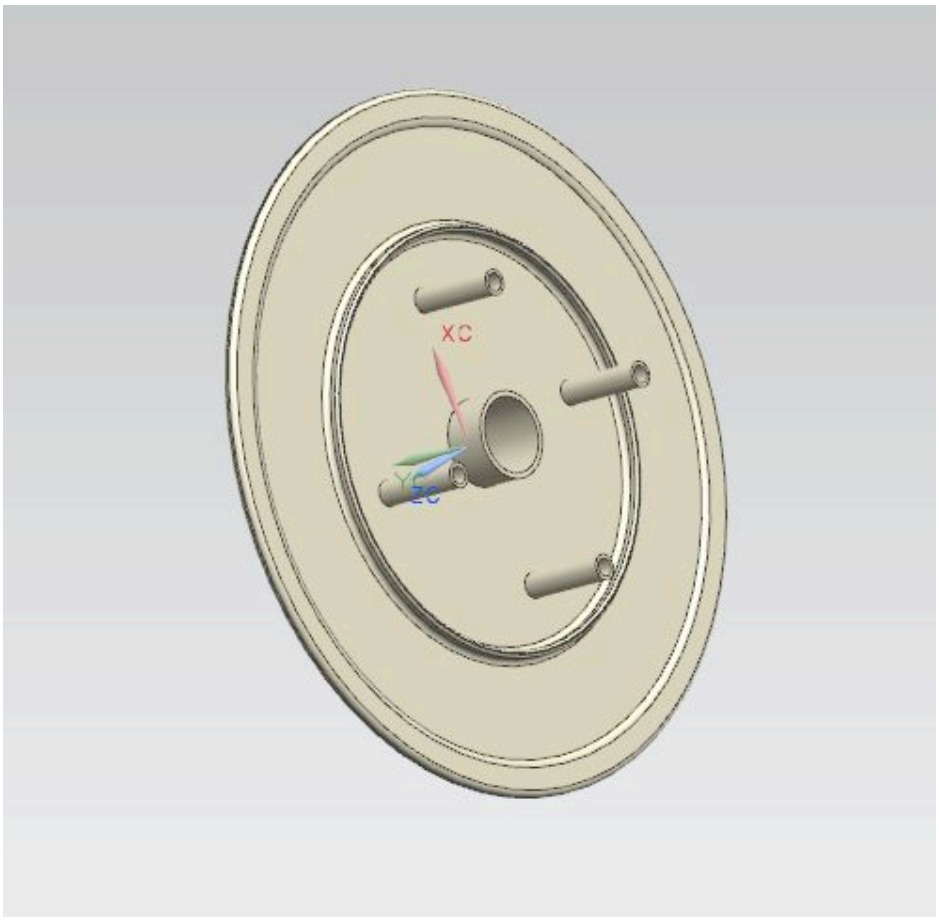

Figure 25. CAD Model for a Single Picker Disk

The force acting upon the picker disk was estimated by using an equation normally associated with determining the max displacement of a cantilever beam. This was applied to the disk by assuming the center of the disk is non-moving and non-deflective and can be seen in Eq. 7,

$$\delta_{\max} = \frac{PL^3}{3EI} \tag{7}$$

where P is the force acting upon the disk, L is the radius of the disk, or 6 in, I is the moment of area of the disk, or 1/512 in^4, and $\delta_{\max}$ is the max displacement of the disk and was determined experimentally to be 1/8 of an inch. The material of the disk was assumed to be ABS, with E

equal to $0.16*10^6$ psi. The above quantities were used to solve for the force, *P,* which was found to be 0.54 lb-f, with a resulting max moment of 3.246 lb-in. Using the known forces, moments, and displacements, Eq. 8 can be used to solve for the change in angle,

$$\begin{bmatrix} f_1 \\ m_1 \\ f_2 \\ m_2 \end{bmatrix} = \frac{EI}{L^3} \begin{bmatrix} 12 & 6L & -12 & 6L \\ 6L & 4L^2 & -6L & 2L^2 \\ -12 & -6L & 12 & -6L \\ 6L & 2L^2 & -6L & 4L^2 \end{bmatrix} * \begin{bmatrix} d_1 \\ \phi_1 \\ d_2 \\ \phi_2 \end{bmatrix} \tag{8}$$

where f_1 and m_1 are reaction forces and moments, f_2 and m_2 are 0.54 lb-f and 3.246 lb-in respectively, d1 is the change in displacement at the center of the disk and is assumed to be zero, ϕ_1 is the change in angle at the center of the disk and is assumed to be zero, d_2 is unknown, and ϕ_2 is the change in angle at the edge of the disk. ϕ_2 and d_2 are solved for by using Eq. 8 and found to be 0.0226 degrees and 0.1584 in, respectively. To solve for the stresses, Eq. 4 through 6 are again used with the part being much wider than its height, with *v* being equal to 0.35. The shear strain can be solved for be using Eq. 9,

$$\gamma = \frac{\phi_2}{d_2} \tag{9}$$

and was determined to be 0.143. The stresses seen on the edge of the disk were determined to be

$$\begin{bmatrix} \sigma_x \\ \sigma_y \\ \tau_{xy} \end{bmatrix} = \begin{bmatrix} -4420.8\,psi \\ -3304.9\,psi \\ -4649.7\,psi \end{bmatrix}$$

NX was again used to perform a more complex FEA analysis on the disk, with the results shown in Figure 26,

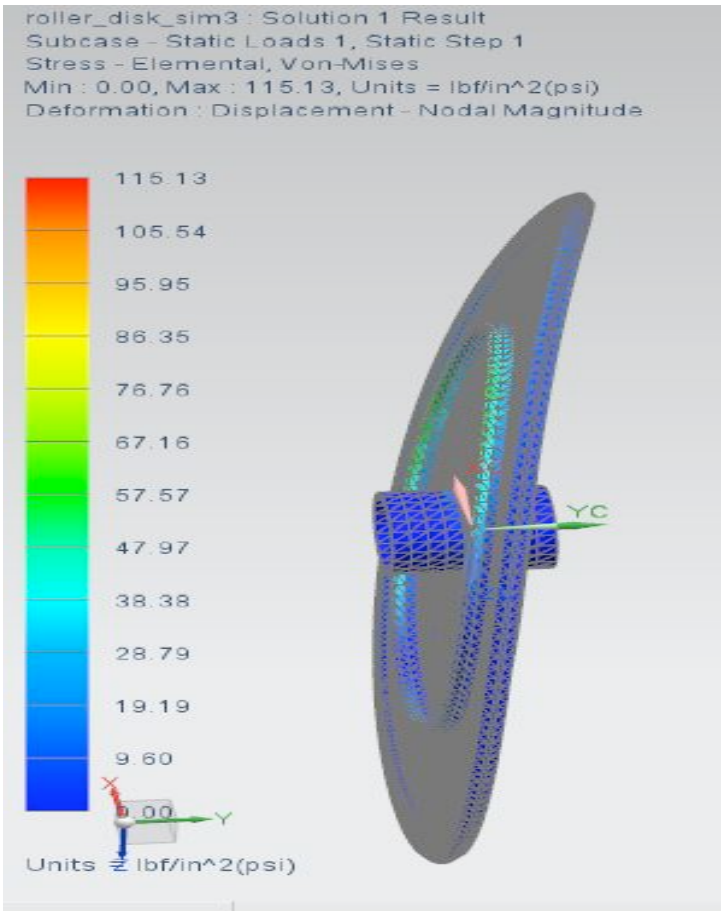

Figure 26. FEA Analysis on Disk Through NX

The figure shows that the max stress felt by the ABS disk was 115 psi, magnitudes of orders less then what was calculated by hand. Differences in calculations can be attributed to the inaccuracy of assuming the picker disk as a cantilever beam so that FEA calculations could be performed. This is especially evident in the calculation for the moment of area I, where the assumption of the cantilever beam resulted in a moment of area calculation for a rectangular cross section instead of the circular one seen here. In addition, the calculations assumed the material of the disk was ABS, however the experimental value of the displacement was determined from an unknown plastic. The material of ABS was chosen for its strength and good ability to do well in a number of environments.

FEA Analysis 3.

The third and final FEA analysis examined the tool that would be used to pry the golf balls out of the picker disks. Due to the golf balls having to displace two disks, the force used to insert a golf ball into one disk was multiplied by two, resulting in a force of 1.08 lb-f. Eq. 8 was again used to calculate the displacements of the disk with the part being assumed to be a cantilever beam, with m_1 = 7.56 lb-in, f_2 equal to 1.08 lb, m_2, d_1, and ϕ_1 set to 0, and f_1, d_2, and ϕ_2 set as unknown. The material properties of the part were based of steel, with *E* equal to 30 Mpsi and poisson's ratio set to 0.29. The dimensions of the beam were found to be L=7 in, width equal to 0.8 in, and height equal to 0.75 in. The moment of area was calculated to be 0.0281 in^4. Plugging into Eq. 8, d_2, and ϕ_2 were both found to be 0.000146 in and degrees, respectively. Using Eq. 5, 6, and 9, ε_x, ε_y, and γ were determined to be $-6*10^{-6}$, $2.1*10^{-5}$, and 1, respectively. The stresses were once again calculated using Eq. 4, with resulting stresses calculated to be

$$\begin{bmatrix} \sigma_x \\ \sigma_y \\ \tau_{xy} \end{bmatrix} = \begin{bmatrix} -208.2 psi \\ -21.86 psi \\ 1.15*10^7 \end{bmatrix}$$

NX was again used to solve for the stresses for the CAD model, with the results shown in Figure 27,

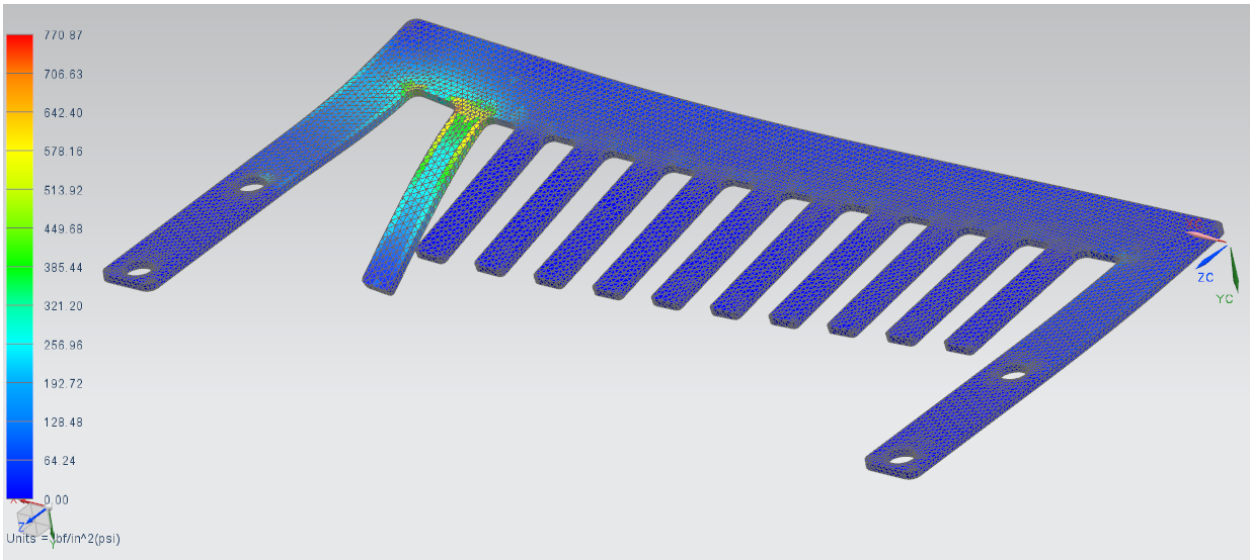

Figure 27. Ball Displacer Stress Analysis

The values calculated are about 2 times greater than the ones found in NX, with a very large shear force recorded. Possible reasons for discrepancies between the two analyzes is that the FEA analysis by hand did not take into consideration the entire ball dislodger part, with more of the stress being able to be distributed throughout the body.

Summary and Future Work

In summary, a golf ball collection system was made that will be able to autonomously collect golf balls on a driving range or golf course. The main components of the collection system can be split into two parts, the Tango E5 robot that performs the path navigation and the golf ball picker trailer that performs the actual golf ball collection. The robot's path navigation will be transferred from the Tango's original purpose (to mow lawns) so that effective and efficient golf ball collection can be performed The golf ball picker trailer consists of hollow rails to provide strength and support, with the actual golf ball collection being performed by golf ball picker disks. The golf ball collection system is a new and novel idea that

will save golf range and golf course owners money, and allow them to spend said profit on things deemed more essential to the business.

Future work on the autonomous golf ball collection system will include providing some method for autonomous removal of golf balls from the storage unit. Current ideas would be to modify the basket so that the golf balls could be funneled out from the basket, or to remove the basket completely and have the golf balls be stored within the robot, eliminating the length of the trailer and using the empty space within the Tango robot. The robot would be provided logic so that upon returning to the charging station, the storage compartment of the golf balls would open and golf balls would be removed. The charging station would also need to be modified to handle this new function. Additionally, FEA analysis would need to be preformed on the storage unit to ensure that stresses caused by the weight of golf balls would not damage the autonomous removal system.